Chemical Vapor Deposition

DOI: 10.1002/cvde.201307057

Full Paper

Design Strategies for Reduced-scale Surface Composition Gradients via CVD Copolymerization**

By *Yaseen Elkasabi, Aftin M. Ross, Jonathan Oh, Michael P. Hoepfner, H. Scott Fogler, Joerg Lahann,* and *Paul H. Krebsbach**

A new method for generating and modeling reduced-scale copolymer gradients by CVD is reported. By exploiting diffusion through confined channels, functionalized [2.2]paracyclophanes are copolymerized into their poly(*p*-xylylene) (PPX) analogues as a composition gradient. Fourier transform infrared (FTIR) and X-ray photoelectron spectroscopy (XPS) are used to verify the gradient composition profiles. Gradients are deposited on both flat substrates and 3-dimensional cylinders. Both the thickness and compositional profiles are fitted to a diffusion-based model using realistic physical parameters. The derived equation can be generalized and optimized for any copolymerization gradient through a confined geometry, thus allowing for broad applicability to other copolymer systems.

Keywords: Coatings, Gradients, Polymers, Surface engineering, Transport modeling

1. Introduction

Technological advancements in engineering and medicine often rely on the formation and utilization of spatiotemporal cues. Many of these approaches mimic the naturally occurring gradients observed in biology. For example, cell migration relies on the presence of signaling gradients that facilitate many in-vivo regenerative processes.[1,2] In addition, chemical surface gradients play a critical role in sensing, mammalian development,[3] tissue regeneration,[2] cell migration,[4] and combinatorial materials discovery.[5] Fabrication of a surface gradient on variable length scales would significantly lower the amount of time required to synthesize a range of surface-coating compositions in series, and place researchers in a position to more accurately replicate normal biological processes.

Several methods of generating surface chemical gradients have been developed over the years.[6] For example, microfluidic methods[7,8] can deliver robust gradients on the micrometer-length scale needed for microbiological environments. Photolithography[9–11] can be used to fabricate reactive chemical and/or surface energy gradients on adjustable length scales; however, the former method can only generate gradients on a fixed length scale; if the gradient slope is to be varied, it is likely to be within a narrow range. Furthermore, three-dimensional gradients on complex objects (e.g., porous scaffolds) are needed for in-vivo applications (e.g., tissue regeneration constructs). This type of robust material complexity cannot be easily realized by currently available photolithographic and/or microfluidic methods. To fill these technological gaps, a surface modification method is needed to preserve the delicate nature of soft materials, as well as the spectrum of complex substrate geometries.

The CVD polymerization process[12,13] conformally coats three-dimensional objects[14] with polymer films at room temperature in a relatively short timeframe, making it an effective system for bio-interfacial applications.[15] Several classes of polymers,[16] such as polynaphthalenes,[17] polyacrylates,[18,19] and polythiophenes[20] can be deposited as thin films with the CVD process. While the CVD of inert PPX has long been used in the micro-fabrication industry,[21,22] the polymerization of their functionalized precursors has been less established.[12,23] The same process can now impart surface coatings with tailored reactivities and functional groups,[24–28] several of which support cell proliferation, growth, and differentiation.[27,29] Recently

[*] Dr. Y. Elkasabi, Prof. P. H. Krebsbach
Department of Biologic and Materials Sciences, University of Michigan School of Dentistry, North Campus Research Complex, 010-A149 2800 Plymouth Ave., Ann Arbor, MI 48109 (USA)
E-mail: paulk@umich.edu
Dr. A. M. Ross, Dr. J. Lahann, Prof. P. H. Krebsbach
Department of Biomedical Engineering, University of Michigan, Ann Arbor, MI 48109 (USA)
Dr. J. Oh, Dr. J. Lahann
Department of Materials Science and Engineering, University of Michigan, Ann Arbor, MI 48109 (USA)
Dr. M. P. Hoepfner, Dr. H. S. Fogler, Dr. J. Lahann
Department of Chemical Engineering, University of Michigan, Ann Arbor, MI 48109 (USA)
Dr. J. Lahann
Department of Macromolecular Science and Engineering, University of Michigan, Ann Arbor, MI 48109 (USA)

[**] The authors would like to acknowledge a NSF major instrumentation grant (DMR-0420785), as well as an NIH T-32 training grant (DE007057-36) and NIH grant (DE018890, PHK). J.L. acknowledges support from DTRA under project HDTRA1-12-1-0039. A.M.R. would also like to acknowledge support from the University of Michigan Rackham Predoctoral Fellowship.

developed methods of gradient-coating deposition use a two-source polymerization of functionalized PPXs.[29,30] The two-source process allows for anisotropic deposition of multiple monomers. By optimizing process conditions, a thin film surface gradient can be formed. We now report an important modification of the CVD gradient process that significantly reduces the gradient slope, an important step towards biomedical applicability of these coatings. This process has also been theoretically modeled and fitted to experimental data, thus providing a means for experimental prediction prior to large-scale production.

2. Results

2.1. CVD Gradient Reduction

Scheme 1 compares the CVD hardware configurations for polymerization and deposition of PPX copolymer coatings. The normal two-source set-up allows for anisotropic deposition of multiple PPXs, compared to the homogeneous copolymerization achieved in the one-source CVD method (Scheme 1a). In the two-source CVD (Scheme 1b), the gradient length scale is dependent on both the mean free path and the mass transport mechanisms. Our strategy was to reduce the length scale of PPX copolymer gradients by eliminating effects due to convection. This was achieved by constructing an apparatus (Scheme 1c) that is placed on top of the substrates, then placing both the substrates and the apparatus in the CVD chamber prior to deposition. The apparatus consisted of a sheet metal baffle erected on top of a poly(dimethylsiloxane (PDMS) mold with millimeter-scale channels cut into the face resting on the substrate (Scheme 1d). Although various channel widths were cut into the mold, all channels held an identical clearance height of 3.3 mm (Scheme 1d). This value was fixed in order to compare opening and length aspect ratios. A sheet metal baffle was erected on top of the mold, with the purpose of segregating and directing monomer flow into opposite sides of the PDMS channels. CVD polymerization was carried out on both silicon and gold substrates attached to the PDMS mold, such that the CVD coatings on the substrates could be analyzed for FTIR and XPS signals after mold removal. Dimers 4-trifluoroacetyl-[2.2]paracyclophane (**1**) and 4-aminomethyl-[2.2]paracyclophane (**2**) were each loaded into a CVD source on opposite sides of the chamber. When transported by argon carrier gas, [2.2]paracyclophanes are thermally cracked into their corresponding quinodimethane structures, which subsequently undergo free-radical polymerization into the corresponding PPXs.

Most of the PDMS channels were wide enough for an FTIR signal to be read after removal of the mold. Results from one representative channel (6.8 mm width) can be found in Figure 1. As the channel path was traversed from one opening to the other (as indicated by distance from source 1 channel opening), the ratio of characteristic IR peaks gradually changed in intensity. The carbonyl stretch at 1716 cm^{-1} (CO) was most pronounced at 0 mm and only

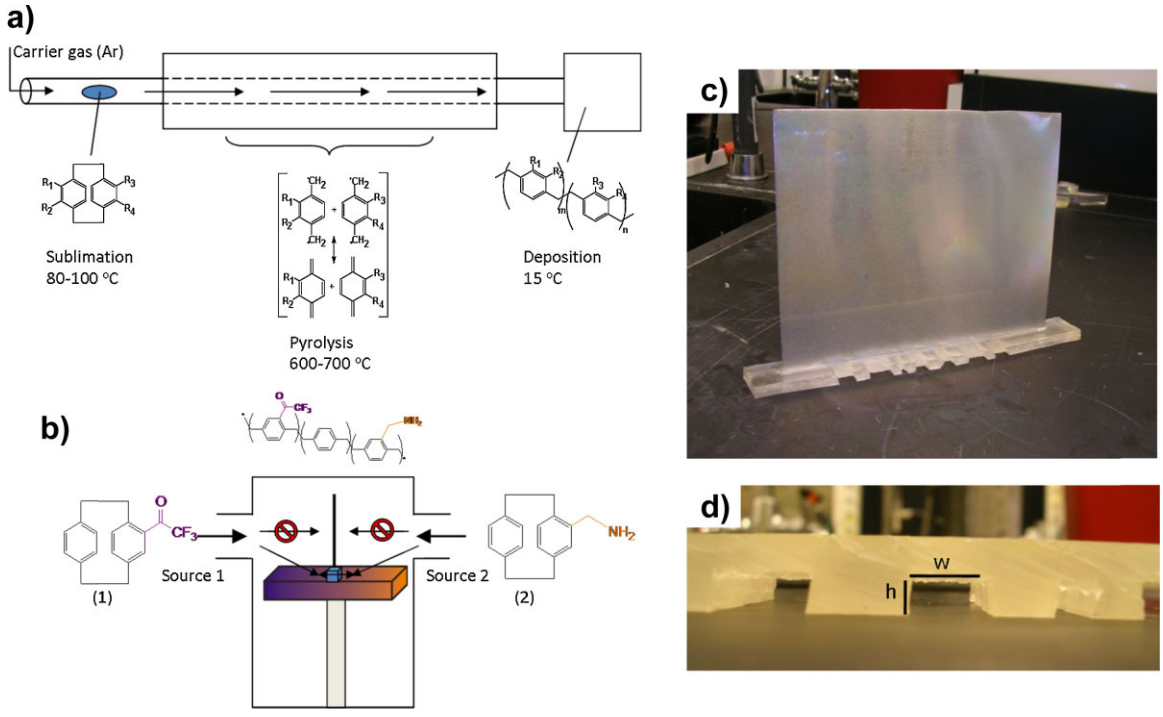

Scheme 1. a) Process diagram depicting one-source CVD polymerization of [2.2]paracyclophane into the corresponding PPX. b) A CVD system with two sources can anisotropically introduce multiple PCPs for deposition of PPX composition gradients. Gradient polymerization and deposition also occurred through PDMS channels joined to a baffle, c) resulting in significantly sharper gradients. d) A magnified view of the labeled channel is shown.

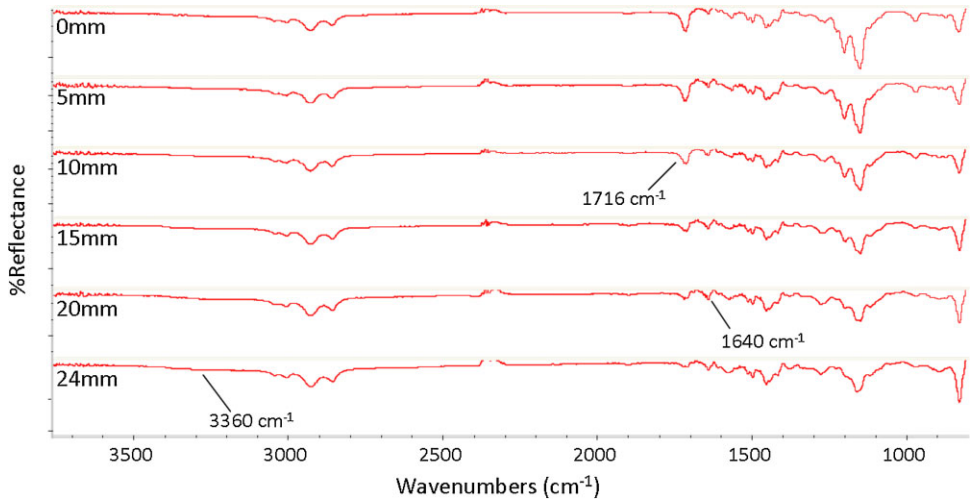

Fig. 1. FTIR spectra, obtained from the PPX composition gradient (channel width $w = 6.8$ mm), reveal a gradual change from predominantly $COCF_3$ to predominantly CH_2NH_2 groups.

decreased in intensity with increasing distance, indicating a decrease in PPX-$COCF_3$ concentration. Likewise, characteristic signal intensities of PPX-CH_2NH_2 (1640, 3300 cm^{-1}) increased as the distance increased from the source 1 channel opening. Even though the bands at 3300 and 3350 cm^{-1} are normally weak, they still exhibited the same gradual increase in intensity (Fig. 2). Thus, the confined channels were capable of reducing the bulk compositional gradient down to a scale smaller than that of the entire CVD system.

Gradient deposition within such a small geometry could bring about strong differences between the bulk film composition and the composition that results on the surface. To assess surface composition, XPS was used to capture the atomistic composition within the top 5–10 nm of the thin film. Fluorine and nitrogen are uniquely indicative of dimers **1** and **2**, respectively, and their compositional ratio directly indicates the copolymer ratio. Figure 3a–c displays compositional profiles for the three different channel widths (3.3 mm, 6.8 mm, and 12 mm). While all three gradient profiles were deposited under the same CVD process conditions, tight control over the slope was maintained. Moreover, the slope of the gradient was inversely proportional to the width of the channel. A homogeneous distribution of functional groups existed perpendicular to the gradient direction, which was also verified by XPS measurements.

Spectroscopic ellipsometry (SE) was used to measure thickness values throughout the channels (Figs. 4a–c). As channel widths increased, the thickness profiles became more uniform, indicating a reduced rate of monomer

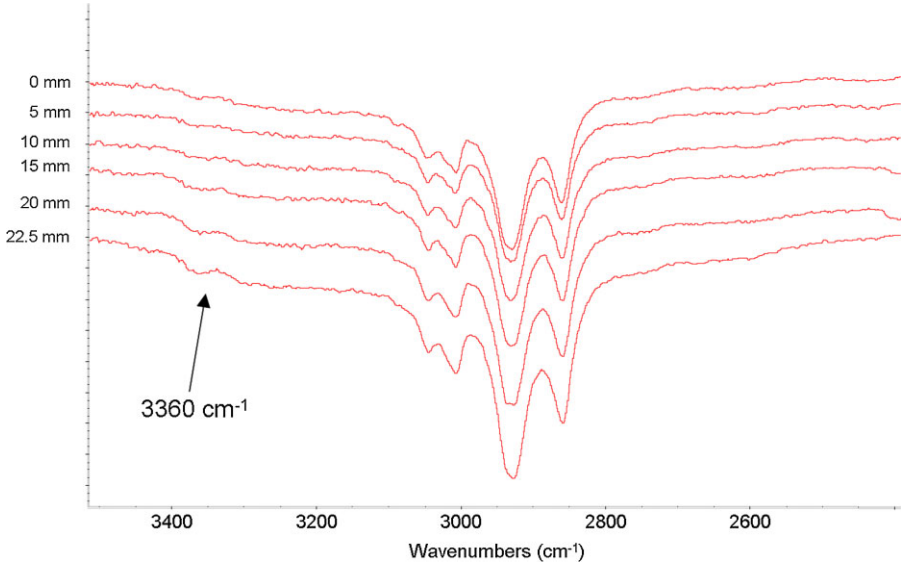

Fig. 2. IR spectra for the polymer gradient, zoomed in on the region containing N-H stretches (arrow). Despite the normally weak band intensities for N–H, the gradient still exhibits a gradual depletion with respect to increasing distance from the channel opening.

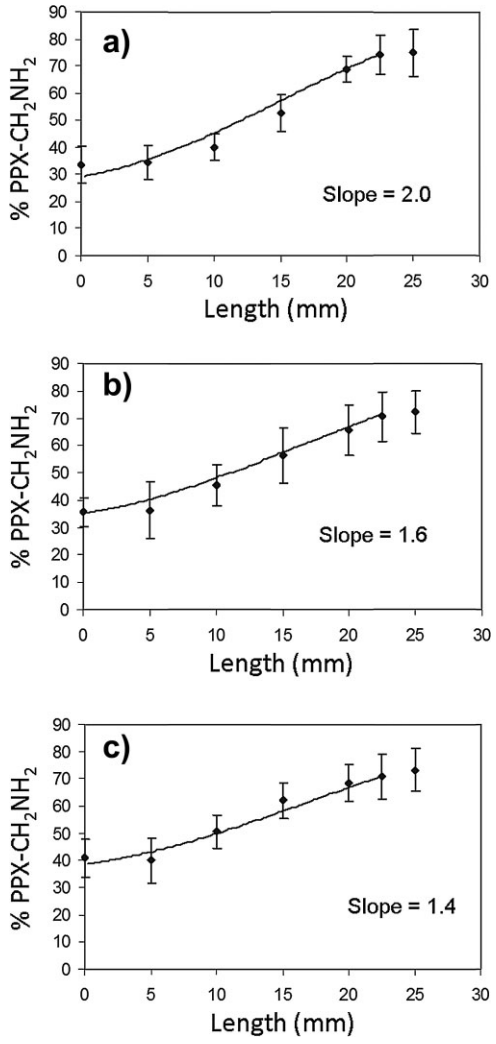

Fig. 3. Copolymer ratios were calculated based on the relative compositions of fluorine and nitrogen from XPS. CVD within rectangular channels $h = 3.3$ mm and a) $w = 3.3$ mm, b) $w = 6.8$ mm, and c) $w = 12$ mm, indicate strong agreement between computational modeling (solid) and experimental (dots) results.

depletion. Thickness profiles from various geometries were compared in a dimensionless coordinate system (Fig. 4d). The thickness values were normalized with respect to the average thickness value t_{av}, to equalize the comparison of topological thickness distributions. When plotted against the dimensionless distance x/L, the plotted profiles showed identical relative rates of change with respect to different channel geometries. Both monomers were consistently deposited at different rates. For all the various channel geometries (width and length), the normalized thickness distribution was identical.

2.2. 3D Deposition

The PDMS channels are capable of closing technological gaps pertaining to both the gradient length and the types of substrates coated. While the PDMS channels significantly reduced the compositional slope of the gradient thin films, they also acted as housing units in which three-dimensional objects were inserted and coated with CVD gradients. 10 μL pipette tips were chosen as a three-dimensional object due to their consistent shape and ability to fit into the channels. The pipette tips were an ideal object of study due to their resemblance to cellular incubators and scaffolds, but also due to their uniform geometry. The tips were sectioned such that the diameters of the open ends were equal ($L = 9$ mm; $ID = 1.0$–1.1 mm; see Fig. 5a). This was done to ensure a direct comparison between the flows on both ends. After splitting the sections in half along the length, the inside coating was analyzed using XPS (Figs. 5b–c). Again, the presence of nitrogen and fluorine were unique indicators of the copolymer ratio. The gradient compositional slope was reduced to an even smaller value than that of the PDMS channel, mostly due to the reduced pipette dimensions. The length over which the gradient occurred (<1 cm) represents more than a tenfold reduction from that of the original CVD gradient method. The compositions at the ends of the pipette tip were similar to that of the gradient in Figure 3a. This result aligns well with our hypotheses because the two channels were identical in aspect ratio. Both have symmetrical cross-sectional geometries (square vs. circle), leading to identical rates of depletion.[31]

3. Discussion

3.1. Derivation of Design Equation

To better predict the gradient film characteristics, we derived a reaction engineering-based model to describe the gradient and compute the thickness and composition profiles. These theoretical values were then compared to values from experimental measurements. Our goal was to model the flow, composition, and thickness topographies, but not the mechanism of polymerization. Thus, only the rate of deposition onto the substrate was considered. Deposition was considered to occur when the monomeric diradical adsorbed onto the film surface, regardless of polymerization spontaneity. Neglecting bulk polymerization in the vapor was also an informed assumption.[32] The Knudsen number ($Kn = \lambda/h$) was calculated to check if the channel flow was characteristic of Knudsen diffusion. For our system, $Kn < 0.1$ indicates the absence of Knudsen diffusion and validity of normal continuum flow theory. Furthermore, flow through the confined channels can be assumed to be purely diffusive. Although the carrier gas contributes to a convective flow, the only streamline present flows directly to the pump. Only a diffusive driving force can transport monomer through any existing boundary layers. The sharp reduction in flow diameter (i.e., the PDMS channel) and the presence of a baffle eliminated convection.

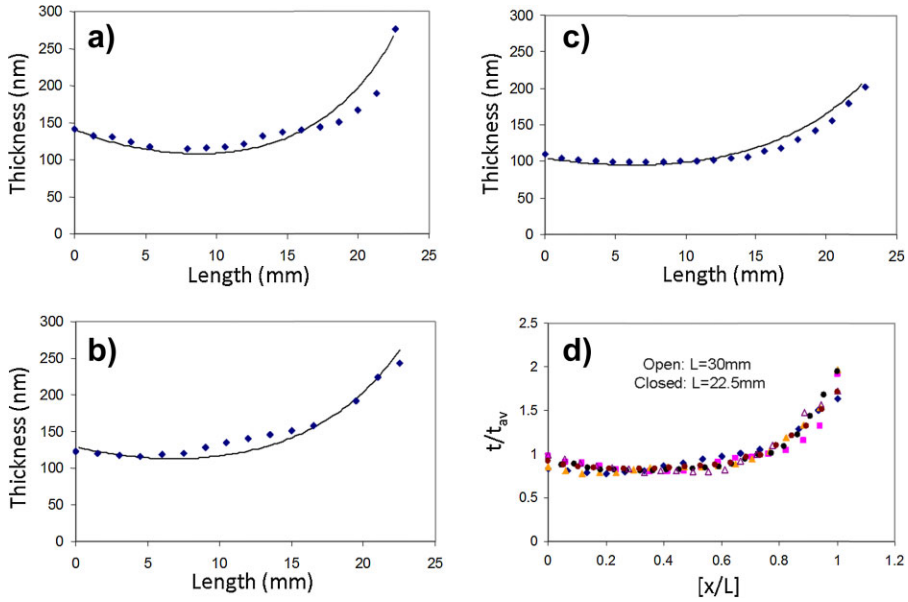

Fig. 4. Ellipsometric thickness profiles of copolymer gradients deposited within varying channel dimensions; a) $w = 3.3$ mm, b) $w = 6.8$ mm, c) $w = 12$ mm. Computational results (solid line) using identical parameters agree well with experimental (dotted) results. d) Six different thickness profiles from various channel dimensions (varying length and width) are plotted in dimensionless form. All thickness profiles are identical when normalized by the channel dimensions and the average thickness.

With respect to wall surface area, different channel geometries will deplete the monomer vapor at different rates. The dimensionless variable, $Z^* = z \cdot \left(\frac{B_c}{A_c}\right)$, equalizes the comparison between these different geometries.[31] Here, z is the distance from the $COCF_3$ monomer entry, B_c is the cross-sectional perimeter, and A_c is the cross-sectional area. When the normalized mole fraction is plotted against Z^* (Fig. 6), all the compositional plots (Figs. 4a–c and Fig. 55c) become identical and superimposed, showing that geometry is the only variable that contributes to the disappearance of monomer (versus diffusion through PDMS or possible backflow). The trends also verify the accuracy of the data.

The CVD polymerization of [2.2]paracyclophanes is well known to have transport limitations prior to polymerization, including adsorption limitations.[16,22] Therefore, bulk diffusion in the channel is relatively rapid, and C can be approximated as the average vapor-phase concentration at location z. All variables are given in SI units. Scheme 2 illustrates the derivation for the shell balance on the channel, a necessary step for deriving the design equation. Molecular flux due to diffusion occurs through the channel cross-sectional

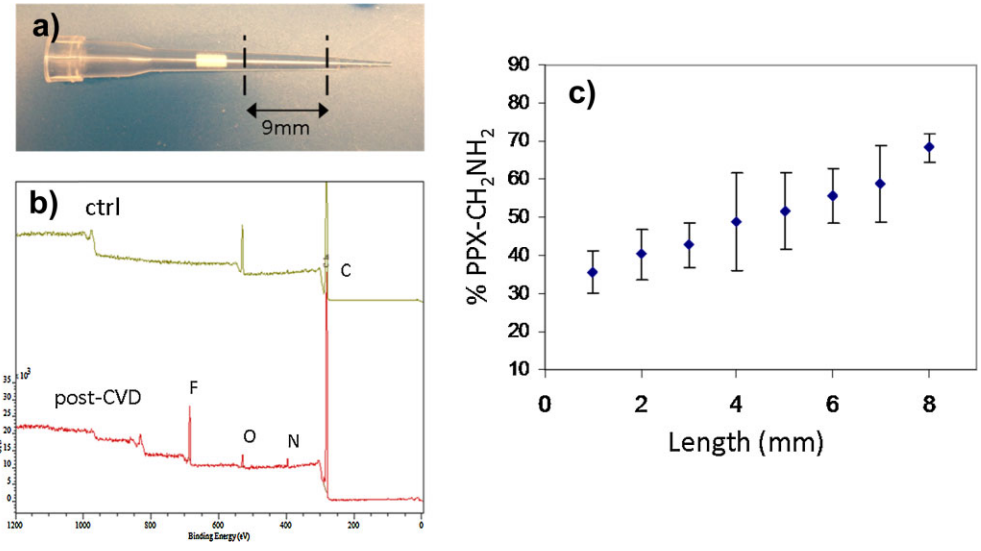

Fig. 5. a) Pipette tips that were sectioned and inserted into the amended CVD apparatus. b) XPS survey scans at one location inside the pipette tip before and after gradient deposition. c) Composition profile on the pipette inner surface post-deposition.

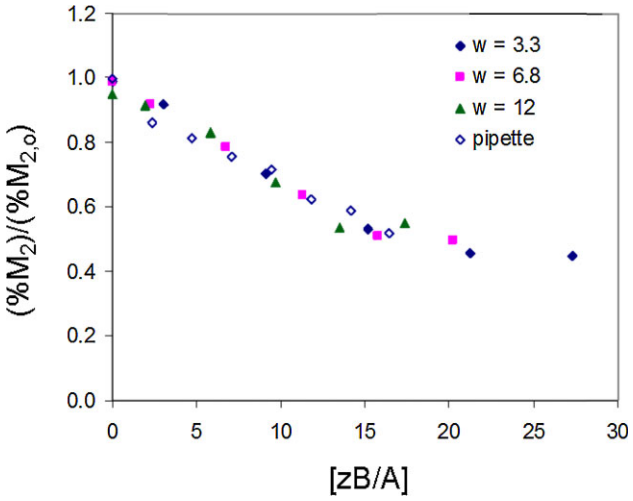

Fig. 6. XPS composition profiles are plotted on a dimensionless coordinate system, where geometrical channel differences have been removed. The plot illustrates that the channel geometry is the only factor which affects the rate of monomer depletion.

area, whereas the flux due to deposition occurs on the inner wall surface. Fick's law of diffusion for a steady-state process (Eq. 1) gives the relationship between molecular flux and concentration, with respect to distance.

$$J_{diff} = -D_i \frac{dC_i}{dz} \tag{1}$$

D_i [$m^2 s^{-1}$] is the diffusivity of monomer i. Compositional differences perpendicular to the flow are assumed to be negligible, and this was shown to be true experimentally as indicated by XPS measurements. Parylene deposition rates have traditionally been modeled as a power-law rate function of concentration at the bare surface.[32] We modeled the depositional flux as a power-law rate relationship, except that $C(z)$ was considered in terms of the average vapor-phase concentration at location z. Taking a mole balance on a differential length (Scheme 2) produces Equation 2.

$$\left(whD_i \frac{dC_i}{dz}\right)_{in} - \left(whD_i \frac{dC_i}{dz}\right)_{out} - \Delta z(2w + 2h)k_i C_i^{\,n} = 0 \tag{2}$$

Dividing both sides by Δz and taking the limit as Δz approaches zero yields Equation 3.

$$whD_i \frac{d^2 C_i}{dz^2} = (2w + 2h)k_i C_i^{\,n_i} \tag{3}$$

w and h represent the width and height of the channel cross-section. The boundary conditions (Eq. 4) and (Eq. 5) are experimentally feasible and accurate, especially in light of Figure 6.

$$C(0) = C_o \tag{4}$$

$$\left(\frac{dC}{dz}\right)_{z=L} = 0 \tag{5}$$

Mass diffusivities can be calculated from Equation 6,[34] based on ideal gas behavior.

$$D_i = \frac{2\sqrt{\pi m_i k_B T}}{3\rho(\pi d_i)^2} \tag{6}$$

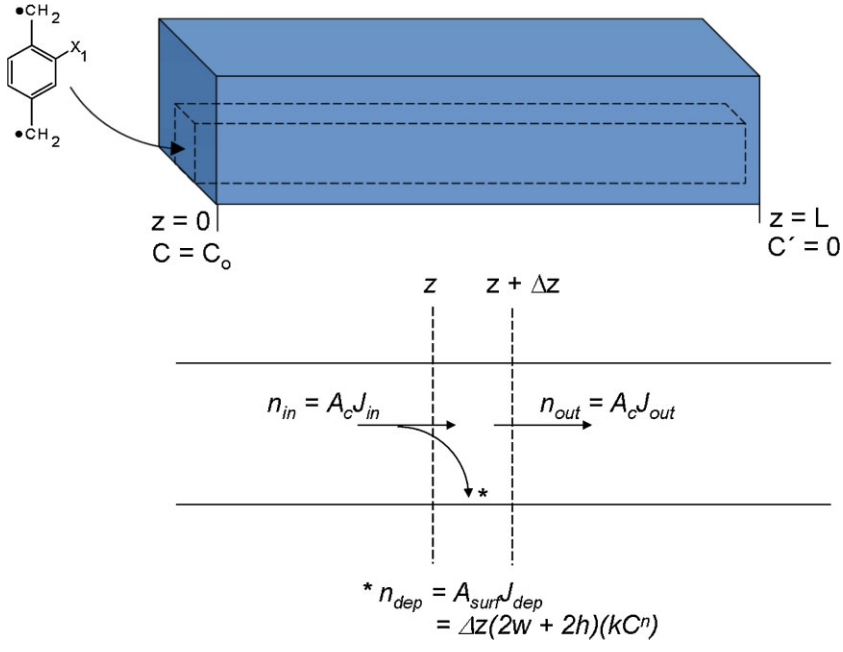

Scheme 2. The shell balance used for derivation of the process design Equation 3.

3.2. Computation and Optimization

Although D_i is calculated, the actual value will exhibit a deviation from the theoretical calculation. Hence, D_i and C_0 remain adjustable variables along with n and k. Alongside these 4 variables, there exist 4 experimental constraints on the design equation, namely: the composition ratio measurements from XPS, the polymer deposition rate measurements from in-situ quartz crystal microbalance, the film thickness measurements from ellipsometry, and $n = 1.5$. The first three constraints are a result of independent experimental measurements. Hence, all of these constraints together determine k_i. Numerical computations were carried out using MATLAB. Since the CVD vapor concentration is fundamentally anisotropic, the chamber partial pressure ($P_{M,avg}$) approximation for $C_{0,i}$ will be inaccurate. Approximately 3–5% of the loaded monomer deposits onto the target sample(s), so we used this ratio as a first approximation for $C_0/C_{chamber}$. The ratio of $C_{0,2}/C_{0,1}$ is also set by the monomer sublimation rates, $\dot{m}_2/\dot{m}_1$. Equation 3 was also applied to monomer **2**, except that the boundary conditions were reversed to reflect the opposite entryway. Total thickness of the copolymer was assumed to be additive ($t_{total} = t_{M1} + t_{M2}$) and based upon the vapor-phase concentration power law. Converting the surface flux into a deposition rate produces Equation 7, in which τ is the deposition time.

$$t_{total}(z) = \sum_i \frac{k_i C_i(z)^{n_i} \tau M_i}{\rho} \tag{7}$$

The copolymer ratio can be calculated based upon t_1 and t_2, since the surface composition was demonstrated to be very close to that of the bulk.[35] The reaction rate order n_i is assumed to be 1.5, based upon the model of the polymer film as a bulk diffusion reaction.[33] When using the first-approximation values for D_i and $C_{0,i}$, both the thickness and compositional curves come to be within very close range of the experimental curves. Figures 3 and 4 compare the experimental and theoretically calculated composition and thickness distributions, after optimization by adjusting D_i, C_0, and k_i. The parameter values used for each of the three geometries investigated were nearly identical and fell within approximately one standard deviation from the mean (Table 1). Thickness calculations were very sensitive with respect to C_0, which helped to fix C_0. Also, D_i must be constrained such that it falls within range of the theoretical calculation. Within this range, varying D_i will change the gradient slope for the particular monomer, although the change is not as dramatic as varying C_0. Values for k_1 and k_2 should be very similar since the mechanism for deposition is nearly identical. The same is true for n_1 and n_2. We find that $k_2 > k_1$, which is consistent with basic structural analysis. The NH_2 group in **2** possesses greater polarity, which increases the driving force for deposition by lowering the adsorption activation energy.[22] Furthermore, we find that $D_2 < D_1$, with respect to both experimental and computational data, thus adding to the difficulty of **2** channel diffusion. According to Equation 6, D_2 should be greater than D_1, but this discrepancy is likely due to a higher local pressure for **2**.

Table 1. Fitted parameters for computation of the thickness and composition profiles produced from the specified CVD process conditions.

	$COCF_3$ (1)	CH_2NH_2 (2)
D_i [$m^2\ s^{-1}$]	0.024	0.011
C_o [$mol\ m^{-3}$]	2.72×10^{-5}	4.70×10^{-5}
n	1.5	1.5
k	11	17

When using a bulk film diffusion model with Flory's surface concentration,[33] the calculated value for k in the literature for unfunctionalized PPX equals 0.5–0.6 $m^{2.5}\ mol^{-0.5}\ s^{-1}$. This value is approximately one order of magnitude lower than the fitted k values (Table 1), and this difference reflects the differences in sticking coefficient that are observed experimentally. Any functional groups added to the PPX chain will add significant polarity and mass, which significantly decreases the adsorption activation energy.[22] Thus, the differences conform with expected values and trends. Furthermore, when using the fitted parameters, the deposition rate is calculated to be 13–15 Å s^{-1}, which agrees very well with the experimentally measured rate of 8–10 Å s^{-1}. Although these deposition rates are higher than the typical CVD operation, they are not uncommon in various CVD polymerization processes.[16] Because PDMS is semi-permeable, some vapor diffusion into the PDMS pores will cause excess monomer depletion. In order for CVD runs to be reproducible and efficient, the PDMS should be used for a few depositions before they are used to produce gradients within the channels. The first few depositions would form a seal over the PDMS pores, hence preventing loss of monomer from the vapor. This is also necessary in order to obtain consistent thickness values. Alternatively, an impermeable material or a mold sealant can be used.

3.3. Generalization of Design Equation

Transforming C and z into dimensionless variables allows for a broad analysis of copolymer gradient coatings with respect to process variables.[36] C is normalized by the monomer concentration at the opening $z = 0$, and z is normalized by the channel length L, as given by Equation 8.

$$\hat{C}_i = \frac{C_i}{C_{i,o}};\ \hat{z} = \frac{z}{L} \tag{8}$$

These variables can then be substituted into Equation 3, yielding Equation 9.

$$\frac{d^2\hat{C}_i}{d\hat{z}^2} = \Phi \hat{C}_i^{\,n};\quad \hat{C}(0) = 1;\quad \left(\frac{d\hat{C}}{d\hat{z}}\right)_{z=1} = 0 \tag{9}$$

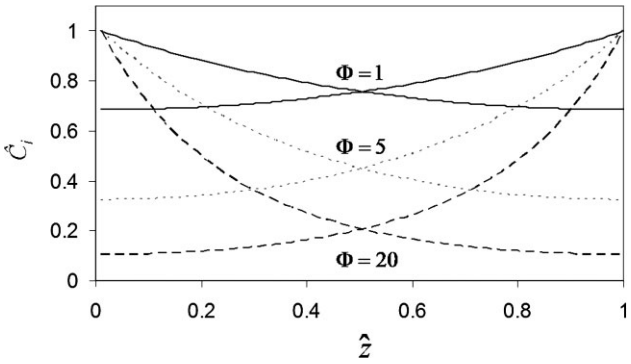

Fig. 7. Dimensionless concentration profiles versus dimensionless channel length, based on calculations of the dimensionless design Equation 9 for various values of the Thiele modulus, $\Phi = 1$ (solid), $\Phi = 5$ (grey dotted), and $\Phi = 20$ (dashed).

Φ is a dimensionless constant given by Equation 10.

$$\Phi = \frac{(2w + 2h)kC_o{}^n L^2}{whDC_o} = \frac{L^2(2w + 2h)}{wh}\frac{R_{d,o}}{D_i C_{o,i}} \quad (10)$$

Φ represents the Thiele modulus for pore diffusion and reaction. All experimental variables relating to both the channel geometry and the CVD process are contained in Φ. Thus, optimization of the gradient deposition involves modification of the process until a suitable value for Φ emerges. Since Equation 9 models a deposition reaction, Φ determines the balance between a sharp gradient and an even thickness distribution. When comparing curves for various values of Φ (Fig. 7), a value of $\Phi = 5$–10 would yield both a wide concentration range and a relatively even thickness, provided that $\Phi_1 = \Phi_2$.

4. Conclusions

In summary, we demonstrated and modeled a method for generating reduced-scale surface composition gradients onto both flat and 3D substrates via CVD copolymerization. The method bypasses transport limitations by exploiting monomer diffusion through confined geometries. Results from FTIR spectroscopy and XPS illustrate the presence of a copolymer gradient in both the bulk film and the surface, respectively. The gradient slope can be adjusted by changing the channel dimensions. A simple Fickian diffusion model accurately predicts the thickness and composition profiles across various channel geometries. With regards to the design equation, adjusting the monomer sublimation rate will directly impact the channel entry concentration. The monomer diffusivity is affected by the carrier gas flow rate. The surface-to-volume ratio of the channel has the most direct effect on the steepness of the composition gradient. All CVD process parameters are stored in the Thiele modulus, a dimensionless constant that indicates both the thickness and compositional uniformities of the gradient. The results reported can be used to better predict new types of CVD gradient coatings on varying length scales, a necessary tool for bridging small-scale biological gradients with complex geometries.

5. Experimental

Apparatus Construction (Scheme 1): PDMS and a curing agent (Sylgard, Dow Corning) were thoroughly mixed, degassed, and poured into plastic wells with an area wide enough to cover the width of the CVD sample holder (20 cm). After thermal curing for 40 min, the PDMS slab was removed, and channels were measured and cut into the underside of the slab. To accommodate a sheet metal baffle, a slit was cut down the center, along the length of the PDMS, with the channel length perpendicular to the slit. The PDMS construct was placed on top of 2 or 3 large silicon pieces, such that no gaps existed between the PDMS and sample holder. Before inserting the baffle into the PDMS, the PDMS/substrate construct was placed on the sample holder, approximately halfway between source 2 and the sample holder midpoint. After inserting the baffle into the slit, tape was used to fasten the baffle to the top of the CVD chamber. Objects for 3D gradient deposition (ART 10 Reach pipette tips, Molecular Bioproducts) were sectioned and inserted into the $w = 6.8$ mm channels, such that the sectioned pipette tips lay entirely within the channel and parallel to the length. After CVD processing, the PDMS slab was removed for characterization of the substrate coating. Pipette tips were then cut in half lengthwise for surface characterization.

CVD Copolymerization: A custom-built, two-source CVD system was used to pyrolyze functionalized [2.2]paracyclophanes for deposition and copolymerization into functionalized PPXs, as depicted in Scheme 1 and described elsewhere [30]. Briefly, **1** and **2** were each loaded into glass dishes in separate quartz tubes, each tube encased in a tube furnace. Each tube feeds into the same chamber on opposite sides 180° from each other. Argon carrier gas was allowed to flow through each tube and into the chamber during dimer sublimation. Pyrolysis temperatures of 670°C were used for each furnace, the sample holder was set to 15°C, and a chamber wall temperature of 110°C was used. Process conditions for CVD copolymerization consisted of the following – dimer loading: $M_1 = 160$ mg, $M_2 = 205$ mg; carrier gas flow rates: $Ar_1 = 6.0$ sccm, $Ar_2 = 27$ sccm.

Surface Characterization: IR spectroscopy was performed on a Nicolet 6700 spectrometer utilizing the grazing angle accessory (Smart SAGA) at a grazing angle of 85°. FTIR spectra were corrected for any residual baseline drift. Au-coated Si substrates were used for FTIR measurements, using blank Au-coated Si as a reference. XPS spectral data were recorded on an Axis Ultra X-ray photoelectron spectrometer (Kratos Analyticals, UK) equipped with a monochromated Al Kα X-ray source. All spectra were calibrated with respect to the non-functionalized aliphatic carbon (BE = 285.0 eV). Thickness measurements were taken using a multi-wavelength imaging null-ellipsometer (EP3 Nanofilm, Germany). Measurements were taken from along the length of a sample in 5 mm increments. At each position, a measurement of delta and psi over a wavelength range of 401.4 nm to 1001.7 nm was taken. Fixed values of the real refractive index, n, of the polymer coatings, along with the measurements of ellipsometric delta and psi, were inserted into an *n_k* fix model to determine film thickness. Values of n were 1.54 and 1.49 for PPX-$COCF_3$ and PPX-CH_2NH_2 coatings, respectively.

Received: January 24, 2013
Revised: May 8, 2013

[1] J. Mey, G. Brook, D. Hodde, A. Kriebel, *Biomed. Appl. Polym. Nanofibers* **2012**, *246*, 131.
[2] C. M. Nelson, J. P. Gleghorn, *Annu. Rev. Biomed. Eng.* **2012**, *14*, 129.
[3] R. Zeller, J. Lopez-Rios, A. Zuniga, *Nat. Rev. Genet.* **2009**, *10*, 845.
[4] D. Irimia, *Annu. Rev. Biomed. Eng.* **2010**, *12*, 259.
[5] M. J. Fasolka, C. M. Stafford, K. L. Beers, *Polym. Libr.* **2010**, *225*, 63.
[6] J. Genzer, R. R. Bhat, *Langmuir* **2008**, *24*, 2294.
[7] B. G. Chung, J. Choo, *Electrophoresis* **2010**, *31*, 3014.
[8] D. B. Weibel, G. M. Whitesides, *Curr. Opin. Chem. Biol.* **2006**, *10*, 584.
[9] N. Ballav, A. Shaporenko, A. Terfort, M. Zharnikov, *Adv. Mater.* **2007**, *19*, 998.
[10] W. S. Dillmore, M. N. Yousaf, M. Mrksich, *Langmuir* **2004**, *20*, 7223.
[11] P. Burgos, M. Geoghegan, G. J. Leggett, *Nano Lett.* **2007**, *7*, 3747.
[12] J. Lahann, *Polym. Int.* **2006**, *55*, 1361.

[13] R. Sreenivasan, K. K. Gleason, *Chem. Vap. Deposition* **2009**, *15*, 77.
[14] P. D. Haller, C. A. Flowers, M. Gupta, *Soft Matter* **2011**, *7*, 2428.
[15] H. Y. Chen, J. Lahann, *Langmuir* **2011**, *27*, 34.
[16] M. E. Alf, A. Asatekin, M. C. Barr, S. H. Baxamusa, H. Chelawat, G. Ozaydin-Ince, C. D. Petruczok, R. Sreenivasan, W. E. Tenhaeff, N. J. Trujillo, S. Vaddiraju, J. Xu, K. K. Gleason, *Adv. Mater.* **2010**, *22*, 1993.
[17] C.-I. Lang, G.-R. Yang, J. A. Moore, T.-M. Lu, *Mater. Res. Soc. Symp. Proc.* **1995**, *381*, 45.
[18] R. K. Bose, K. K. S. Lau, *Chem. Vap. Deposition* **2009**, *15*, 150.
[19] M. Gupta, V. Kapur, N. M. Pinkerton, K. K. Gleason, *Chem. Mater.* **2008**, *20*, 1646.
[20] S. Nejati, K. K. S. Lau, *Langmuir* **2011**, *27*, 15223.
[21] W. Gorham, *J. Polym. Sci. A-1* **1966**, *4*, 3027.
[22] J. B. Fortin, T. M. Lu, *Chemical Vapor Deposition Polymerization: The Growth and Properties of Parylene Thin Films*, Kluwer Academic Publishers, Dordrecht, The Netherlands **2004**.
[23] Y. Elkasabi, J. Lahann, in: *Biological Microarrays: Methods and Protocols*; (Eds: A. Khademhosseini, K. Y. Suh, M. Zourob), Humana Press Inc, Totowa, NJ **2011**.
[24] J. Lahann, R. Langer, *Macromolecules* **2002**, *35*, 4380.
[25] H. Nandivada, H. Y. Chen, L. Bondarenko, J. Lahann, *Angew. Chem. Int. Ed.* **2006**, *45*, 3360.
[26] A. K. Bier, M. Bognitzki, A. Schmidt, A. Greiner, E. Gallo, P. Klack, B. Schartel, *Macromolecules* **2012**, *45*, 633.
[27] M. Y. Tsai, C. Y. Lin, C. H. Huang, J. A. Gu, S. T. Huang, J. Yu, H. Y. Chen, *Chem. Commun.* **2012**, *48*, 10969.
[28] D. Frank, M. Nieger, C. Friedmann, J. Lahann, S. Brase, *Isr. J. Chem.* **2012**, *52*, 143.
[29] Y. Elkasabi, J. Lahann, P. H. Krebsbach, *Biomaterials* **2011**, *32*, 1809.
[30] Y. Elkasabi, J. Lahann, *Macromol. Rapid Commun.* **2009**, *30*, 57.
[31] E. M. Tolstopyatov, *J. Phys. D: Appl. Phys.* **2002**, *35*, 1516.
[32] W. F. Beach, *Macromolecules* **1978**, *11*, 72.
[33] S. Rogojevic, J. A. Moore, W. N. Gill, *J. Vac. Sci. Technol. A* **1999**, *17*, 266.
[34] R. B. Bird, W. E. Stewart, E. N. Lightfoot, *Transport Phenomena*, *2nd ed.* John Wiley & Sons, Inc, New York **2002**, pp. 526.
[35] Y. Elkasabi, H. Y. Chen, J. Lahann, *Adv. Mater.* **2006**, *18*, 1521.
[36] A. Ramachandran, M. Junk, K. P. Koch, K. P. Hoffmann, *IEEE Trans. Adv. Packag.* **2007**, *30*, 712.

